Chimeralike oscillation modes in excitable scale-free networks

Zhao Lei [ORCID],[1,2] Chi Zhang,[1,2] Yafeng Wang,[1,2] Zegang Wei,[1,2] Yu Qian,[1,2,*] and Zhigang Zheng [ORCID][3,4,5,†]

[1]*College of Physics and Optoelectronic Technology, Baoji University of Arts and Sciences, Baoji 721007, China*
[2]*Advanced Titanium Alloys and Functional Coatings Cooperative Innovation Center, Baoji 721007, China*
[3]*Institute of Systems Science, Huaqiao University, Xiamen 361021, China*
[4]*School of Mathematical Sciences, Huaqiao University, Quanzhou 362021, China*
[5]*College of Information Science and Engineering, Huaqiao University, Xiamen 361021, China*

A topological mechanism of the emergence of *chimeralike oscillation modes* (CLOMs) consisting of coherent synchronous firings and incoherent nonsynchronous oscillations is proposed in *excitable scale-free networks* (ESFNs). It is revealed that the topology heterogeneity of the network is responsible for forming and maintaining the CLOM in the ESFN, which is definitely different from the mechanism of the *normal oscillation mode* (NOM) possessing only a single dynamical mode in homogeneous excitable systems. An effective-driving approach is proposed, which provides a criterion for the formation of the CLOM in excitable complex networks. Our contributions may shed light on a perspective of CLOMs in complex systems, and can help us understand competitions and self-organizations of NOM and CLOM in excitable systems with topological homogeneity and heterogeneity.

I. INTRODUCTION

An excitable cell is ubiquitous in nature [1,2], such as in physical, chemical, and biological systems, for typical examples. It can implement a perfect spiking as stimulated by a suprathreshold excitation. Although a single excitable unit is dynamically passive and nonoscillatory, collectively permanent spatiotemporal behaviors can self-organize to emerge in complex excitable systems. Experimentally, researchers have confirmed that self-sustained oscillations do exist in actual biological systems consisting of excitable cells, especially in neuronal networks and brain systems, and are closely related to some vital physiological processes [3–6]. Theoretically, the mathematical model of an excitable complex network has been set up to carry out investigations on these issues, and lots of interesting and important results have been obtained in recent decades [7–14]. For example, sustained activities and synchronous firings were reported in small-world networks consisting of excitable units [7–9]. The propagation problems of excitable waves were studied in Refs. [11,12]. Complex self-sustained oscillation patterns were exposed in modular excitable networks [14]. We have performed extensive studies on this topic in recent years and proposed the *dominant phase-advanced driving* (DPAD) approach to explore the

mechanism of sustained oscillations on networks of excitable units. Specifically, we revealed the self-sustained target-wave-group patterns and the corresponding transitions in excitable small-world networks [15], the emergence of oscillations in excitable Erdös-Rényi (ER) random networks [16], the Winfree loop sustained oscillations in 2D lattices consisting of excitable units [17], the optimal oscillation mode and its dynamical transition in excitable complex networks [18,19], and the burst-oscillation mode in paced one-dimensional excitable systems [20].

Chimera is a spatiotemporal oscillatory state consisting of both coherent and incoherent clusters [21,22]. This phenomenon was reported by Kuramoto and Battogtokh in a nonlocally coupled phase oscillators system [23], which possesses the features of identical local dynamics and a fully symmetric network structure, and can emerge as the spontaneous symmetry breaking. Over the past decades, there has been extensive progress in this field, exhibiting an increasing interest in chimeras. It has been exposed that chimera states can be observed not only in coupled phase oscillators but also in other systems with distinct local dynamics, such as discrete maps [24], continuous chaotic systems [25], bursting neurons [26], bistable models [27], and excitable cells [28]. Chimera states such as breathing chimeras [29], spiral-wave chimeras [30], multichimeras [31], chimera death [32], as well as amplitude and amplitude-mediated chimeras [33] have been revealed. Importantly, in most cases, rotational coupling scheme is considered as the mechanism in forming the chimeras.

With these excellent contributions, the conceptual scope of a chimera state has been extended to systems without topological symmetry, especially in neuronal networks and brain systems, where the phenomenon of chimeralike

---

*qianyu0272@163.com
†zgzheng@hqu.edu.cn

behavior (i.e., the behavior possessing multiple dynamical modes) rather than the symmetry breaking is the focus of exploration. In fact, the mechanism of the chimeralike behaviors beyond the spontaneous symmetry-breaking is still a nontrivial issue because the potential applications of chimeralike behaviors in these living systems are related to many vital physiological processes, such as the unihemispheric sleep of some marine mammals [34], the first-night effect in human sleep [35], and epileptic seizures [36]. Consequently, studies of chimeralike behaviors in these vital complex systems beyond perfectly symmetric structures and the corresponding mechanisms have now become a central topic in the interdisciplinary field of neuroscience and life science [37–41].

Until now, as we know, almost all studies on the issue of chimeralike behaviors in this field have been focused on systems with oscillatory local dynamics, such as the FHN model in the oscillatory parameter region, the Hodgkin-Huxley (HH) neuron with persistent spiking behavior, and the Hindmarsh-Rose neuron with bursting dynamics. Very little attention on chimeralike dynamics has been paid to systems with nonoscillatory local dynamics. It is important to investigate whether similar *chimeralike oscillation modes* (CLOMs, i.e., the oscillations possessing multiple dynamical modes) can self-organize to emerge in complex systems consisting of nonoscillatory excitable units. We have revealed in previous works that, for most homogeneous excitable complex networks, such as ER random networks, homogeneous random networks, and small-world networks, the system possesses the typical *normal oscillation mode* (NOM), i.e., only a single dynamical mode, and the Winfree loop is revealed as the source in maintaining this type of oscillation mode. The CLOM has never been found in these homogeneous systems. For heterogeneous networks, such as *excitable scale-free networks* (ESFNs), both hubs with extraordinarily high degrees and nodes with very low degrees can coexist. This topology heterogeneity of scale-free networks implies a chance to find the oscillations with multiple dynamical modes. So it is valuable to study whether CLOMs can self-organize to emerge in excitable complex networks with topological heterogeneity and the mechanism for this kind of oscillation mode.

In this paper, we propose a topological mechanism giving rise to the CLOM in networks of excitable cells. By exploring the ESFN dynamics, we reveal that the topology heterogeneity of the network plays a key role in forming and maintaining the coexistence of coherent and incoherent motions.

The remainder is organized as follows. The mathematical model and the order parameters are introduced in Sec. II. Section III reports our observation of the emergence of the CLOMs in the ESFNs. In Sec. IV, the corresponding mechanism is discussed in detail. Section V proposes an effective-driving approach to theoretically analyze the emergence of the CLOMs in excitable systems. We give the conclusion in the last section.

II. MATHEMATICAL MODEL AND ORDER PARAMETERS

Let us construct the ESFN dynamics by adopting the Bär-Eiswirth model [42] as the representative excitable dynamics on nodes. In fact, the following discussions and the revealed mechanism in this paper can be naturally realized in excitable networks with other node dynamics. The evolution of the considered ESFN is governed by the following equations:

$$\frac{du_i}{dt} = \frac{1}{\varepsilon}u_i(1-u_i)\left(u_i - \frac{v_i + b}{a}\right) + D\sum_{j=1}^{N}A_{i,j}(u_j - u_i),$$
(1)

$$\frac{dv_i}{dt} = f(u_i) - v_i.$$
(2)

In Eqs. (1) and (2), the subscripts i, j $(i, j = 1, 2, \ldots, N)$ label the nodes in the network, where N is the size of the system. Variables u and v are, respectively, the activation and the recovery variables of the local cell that can imitate the membrane potential and the recovery current of neuronal dynamics. Symbol $f(u)$ represents a piecewise function and follows the form $f(u) = 0$ for $u < \frac{1}{3}$, $f(u) = 1 - 6.75u(u-1)^2$ for $\frac{1}{3} \leqslant u \leqslant 1$, and $f(u) = 1$ for $u > 1$. The three dimensionless parameters a, b, and ε are the characteristic quantities of the Bär-Eiswirth model that can effectively regulate the local dynamics.

The influence of the network structure is described by the diffusion coupling term $D\sum_{j=1}^{N}A_{i,j}(u_j - u_i)$, where D is the coupling strength. $A_{i,j}$ is the adjacency matrix element between any pair of cells (i, j), which is defined as $A_{i,j} = A_{j,i} = 1$ if there is an edge linking cells i and j, and $A_{i,j} = A_{j,i} = 0$ otherwise. The scale-free network in this paper is constructed according to the Barabási-Albert procedure with the characteristic parameters m_0 and m, where m_0 indicates the initial number of cells in the network and m represents the number of edges of the new added cell at each time step [43]. According to the property of the scale-free structure, the average degree can be calculated as $\langle k \rangle = \lim_{N \to \infty} \frac{2[C_0 + m(N - m_0)]}{N} \approx 2m$, with C_0 being the number of edges of the m_0 initial cells. This means that the average degree of a node in a scale-free network approximatively equals to $2m$. More importantly, the links of an ordinary cell are largely connected to the hubs. In the following, we fix node dynamics in the excitable regime by fixing parameters as $a = 0.84$, $b = 0.07$, $\varepsilon = 0.04$, and the coupling strength $D = 0.45$. The scale-free network parameters are set as $m_0 = 2$ and $m = 2$. Initial values of $\{u_i(t=0), v_i(t=0)\}$ $(i = 1, 2, \ldots, N)$ are randomly given between 0 and 1.

To characterize the coherence and incoherent parts of the CLOM, one first introduces the local order parameter Z_i to measure the local phase ordering of the cells as [44]

$$Z_i = \left|\frac{1}{k_i}\sum_{j=1}^{N}A_{i,j}e^{\sqrt{-1}\Phi_j}\right|, \quad i = 1, 2, \ldots, N.$$
(3)

Here k_i is the degree of the ith cell, and Φ_j is the instantaneous phase of the jth unit that can be measured as $\Phi_j = \arctan(v_j/u_j)$. For the coherence domain, the local order parameter $Z_i \approx 1$, while $Z_i < 1$ indicates the incoherent part. To further testify the frequency coherence, the mean phase velocity ω_i is introduced as the long-time average of the phase velocity of each cell, i.e.,

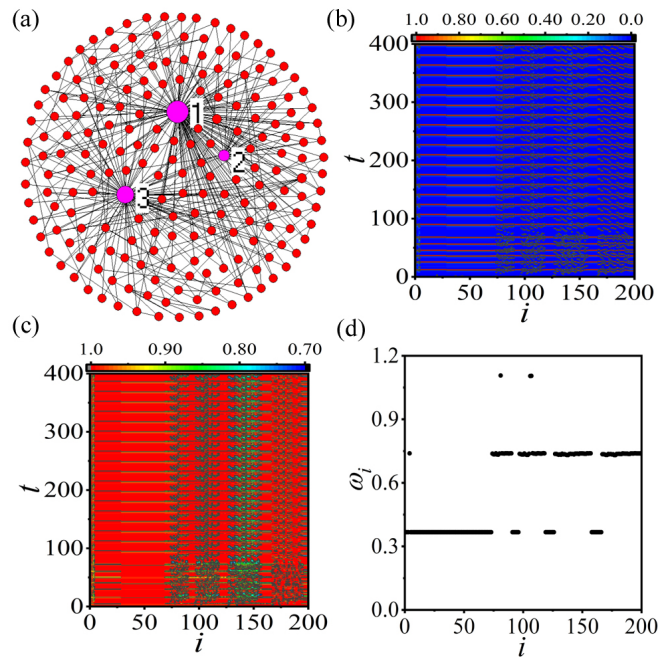$$\omega_i = \frac{2\pi M_i}{\Delta T}, \quad i = 1, 2, \ldots, N.$$
(4)

FIG. 1. (a) A typical *excitable scale-free network* (ESFN) with $N = 200$ cells. The parameters are fixed as $a = 0.84$, $b = 0.07$, $\varepsilon = 0.04$, $D = 0.45$, $m_0 = 2$, and $m = 2$. The three pink nodes $i = 1$, 2, 3 denote the hubs in the network. (b) The *chimeralike oscillation mode* (CLOM) pattern realized in the ESFN of (a) with a suitable set of initial values. (c), (d) The corresponding local order parameter Z_i [(c)] and the mean phase velocity profile $\{\omega_i\}$ [(d)] of the CLOM (b).

In Eq. (4), ΔT is a sufficiently long sampling time interval and M_i denotes the number of excitations of the ith cell during this time interval. The emergence of CLOM in an excitable network can also be implied by the existence of several bands in the frequency profile, while a unique band of $\{\omega_i\}$ indicates a global coherence and furthermore a NOM.

III. CLOMS EMERGING IN THE ESFNS

A typical ESFN with $N = 200$ nodes is constructed and shown in Fig. 1(a). Three hubs labeled by $i = 1$, 2, and 3 in the network are indicated by pink circles. Topology heterogeneity is the unique attribute of a scale-free network. Starting from random initial conditions, different oscillation patterns can be observed. Figure 1(b) exhibits a typical spatiotemporal pattern of sustained oscillation emerging in the ESFN of Fig. 1(a). It is shown that the global dynamics of the network consists of two distinct dynamical modes, where some cells execute coherent synchronous firings (illustrated by the evident lines), while the others perform incoherent non-synchronous oscillations (denoted by the messy dots). One can further observe the spatial profiles of the local order parameter Z_i and the mean phase velocity $\{\omega_i\}$, as shown in Figs. 1(c) and 1(d), respectively. Both order parameters exhibit multiple spatiotemporal behaviors of the cells, indicating that the oscillation pattern shown in Fig. 1(b) is a CLOM consisting of both coherent and incoherent parts.

It is important to study the key factors that can determine the emergence of CLOMs in ESFNs. As we know, network structure is a determinant in deciding the spatiotemporal dynamics of system. In addition, other factors need to be discussed. Here we use the network shown in Fig. 1(a) as our example to carry out this issue preliminarily. We first test the impact of random initial conditions on the emergence of CLOMs. Within $M = 10^4$ samples, 24.51% CLOMs have been observed in the given ESFN. Furthermore, the influence of coupling strength D is also studied. For each D, $M = 10^4$ samples are also performed. It is found that this kind of CLOM can emerge in a broad parameter region of coupling strength (i.e., $0.25 \lesssim D \lesssim 0.70$). Importantly, as D is increased in this region, the emergent probability of CLOMs first increases and then decreases, implying that an optimal coupling strength (around $D \approx 0.55$) may facilitate the emergence of CLOMs in the ESFN.

As we have stated above, the key factor in the formation of chimeras is largely related to the mechanism of a rotational coupling scheme. However, in the case of the CLOM revealed in Fig. 1, one didn't introduce this kind of coupling. This implies that the rotational coupling scheme is not the mechanism in forming the CLOM in our case. We also tested the possibility of parameter-induced CLOMs by adjusting the parameters of node dynamics and coupling strength. Numerical results indicate that the emergence of the CLOM is robust. Moreover, in the absence of rotational coupling scheme, this kind of CLOM cannot emerge in homogeneous networks, such as ER random networks, homogeneous random networks, and small-world networks. Therefore, the CLOM in the ESFN implies a unique mechanism of the topology heterogeneity giving rise to this kind of oscillation mode in scale-free networks.

To reveal the mechanism of the CLOM in the ESFN, it is more tractable to perform a topology reduction of the network by discarding the minor cells in Fig. 1(a) to get a minimal network that preserves the CLOM. The principle of this reduction is that the CLOM should be preserved on a minimal structure and any redundant cells and their corresponding links should be removed as many as possible. By starting from discarding different initial nodes, this reduction scheme may lead to different minimal networks. Figures 2(a)–2(d) present two typical examples. Two reduced minimal networks are, respectively, displayed in Figs. 2(a) and 2(c), with both containing a unique hub and other remaining nodes. Figures 2(b) and 2(d) give the corresponding spatiotemporal patterns observed on these two minimal structures, where one starts from the network structure shown in Fig. 1(a) and the oscillation mode displayed in Fig. 1(b) and switches to the minimal network at $t = 200$. Similar CLOMs to that in Fig. 1(b) can be observed, where the black regions represent the rest state of the discarded cells.

Here we use the case shown in Figs. 2(c) and 2(d) for subsequent discussions, where the minimal scale-free network contains a unique hub and 52 ordinary cells, among which four typical nodes are highlighted by other colours, i.e., the pink hub $i = 3$, the blue and green neighbours of hub $i = 66$ and 75, and the orange hub-distant cell $i = 89$. Figure 2(e) displays the corresponding mean phase velocity profile $\{\omega_i\}$ of the CLOM shown in Fig. 2(d). Two distinct frequency bands
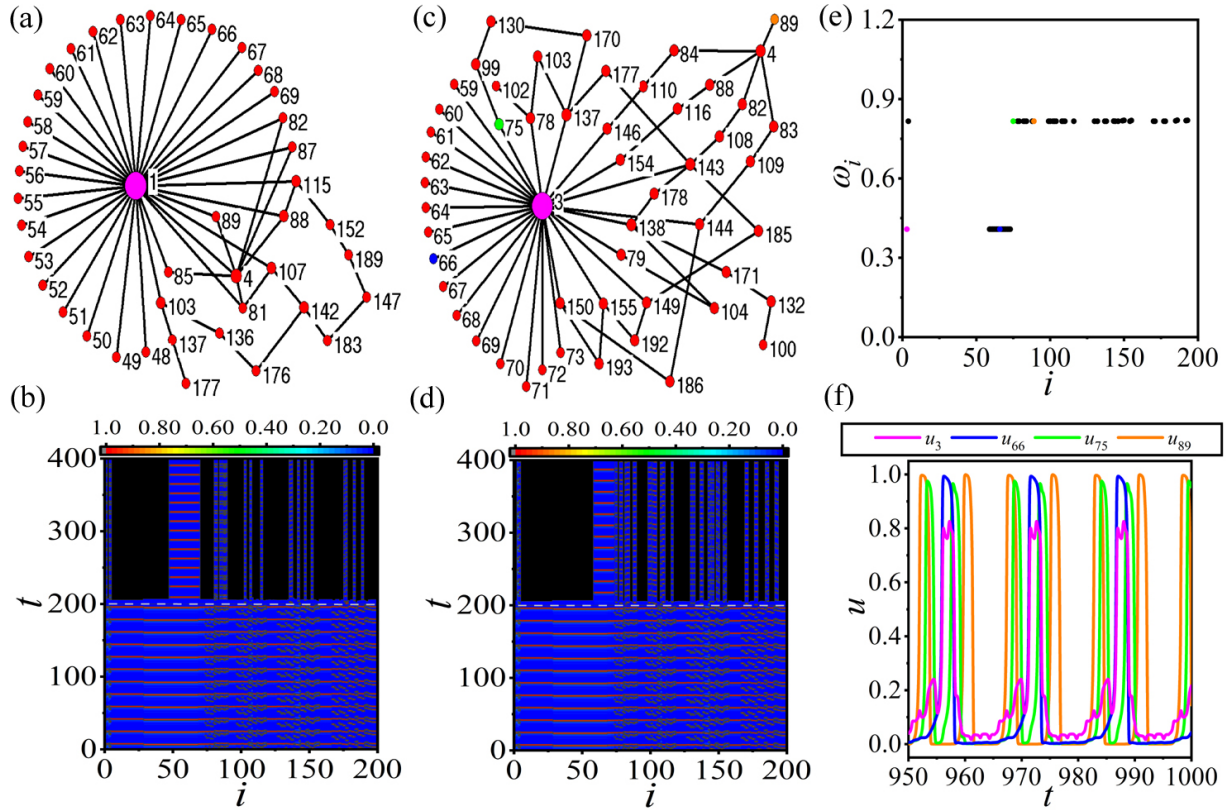
FIG. 2. (a) An example of the minimal network structure with scale-free property containing the unique hub node $i = 1$ that preserves the CLOM by discarding the minor nodes from the original ESFN in Fig. 1(a). (b) The corresponding CLOM pattern preserved on the minimal structure of (a). The reduction is implemented at $t = 200$, which is denoted by the light grey dashed line. The black regions in (b) represent the rest state of the discarded cells. (c), (d) The similar minimal scale-free network with the unique hub node $i = 3$ [(c)] and the CLOM pattern [(d)] as (a) and (b). Four typical cells $i = 3, 66, 75, 89$ in (c) are highlighted by other colours. (e), (f) The mean phase velocity profile $\{\omega_i\}$ [(e)] and the time series of the four highlighted cells [(f)] of the CLOM (d).

can be clearly found, where the constant basic frequency band corresponds to the synchronous coherent part, while the scattered dots around the doubling frequency denote the nonsynchronous incoherent part. The details of the coherent and incoherent dynamics are further shown in Fig. 2(f) by plotting the time series of the highlighted cells in Fig. 2(c). It is shown that the coherent synchronous cells $i = 3$ and 66 excite once in an oscillation period, whereas the incoherent nonsynchronous ones $i = 75$ and 89 can inspire twice. Therefore, a two-mode dynamics with a basic and a doubled frequency is identified on the minimal scale-free topology, which forms the CLOM in the ESFN.

The above discussions indicate that to maintain the CLOM in an excitable network, a minimal network should still possess the topology heterogeneity property. This strongly implies the key role of topology heterogeneity intrinsically rooted in scale-free networks as the mechanism resulting in CLOMs in ESFNs. Moreover, the reduced minimal heterogeneous network provides a convenient platform in excavating the mechanism of this topological-heterogeneity induced CLOM. In the following, we will use the examples revealed in Figs. 2(c) and 2(d) to further discuss in detail how this topological mechanism leads to a coexisting coherent-inherent CLOM.

IV. TOPOLOGICAL MECHANISM OF THE CLOM IN THE ESFN

Because an individual excitable node is dynamically nonoscillatory, a sustained-oscillatory mode as well as the CLOM emerging in the ESFN should originate from topological mechanism of the network. Here we use the DPAD method to explore this issue. The DPAD approach was put forward to expose the mechanism of the persistently oscillatory behaviors in complex networks consisting of nonoscillatory nodes. The central idea and the detailed implementation procedure of the DPAD method have been proposed in our previous contribution [15]. It should be noted that, for the regular oscillation with a single dynamical mode, there only exists a unique DPAD pattern. However, for the CLOM with two spatially distinct dynamical modes, there will be a dynamic alternation between multiple DPAD patterns because of the nonstationary and irregular dynamical property of the incoherent motion. Furthermore, to explicitly reveal the key factor of topology heterogeneity responsible for the formation of the CLOM in the ESFN, all the *phase-advanced drivings* (PADs) of the hub node should be taken into account, while for other ordinary cells, one needs only to plot the corresponding unique DPAD.

Figure 3(a) displays the improved DPAD pattern of the CLOM before the hub node $i = 3$ is excited. It can be clearly
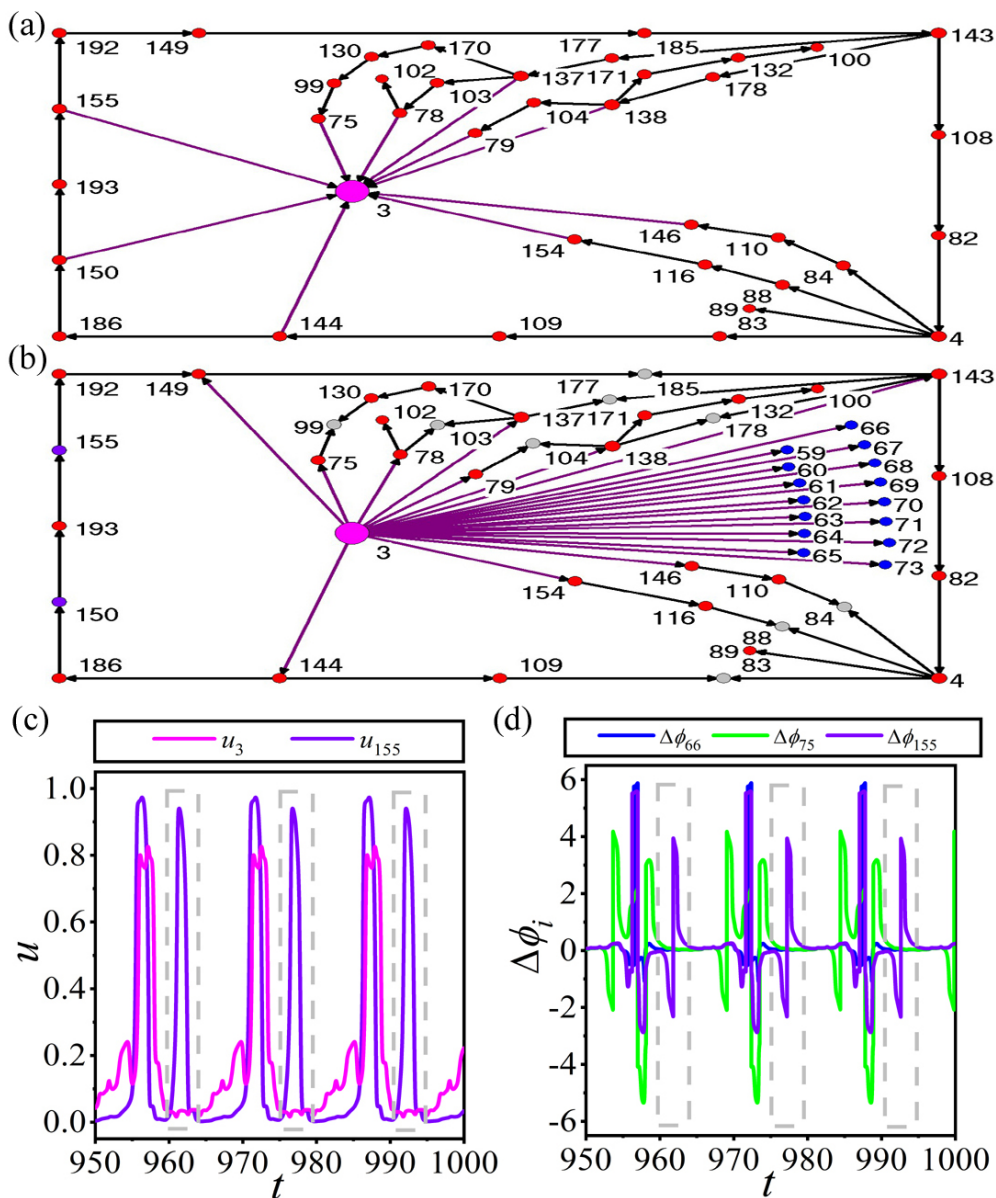
FIG. 3. (a), (b) The improved *dominant phase-advanced driving* (DPAD) patterns of the CLOM of Fig. 2(d) obtained before [(a)] and after [(b)] the hub node $i = 3$ is excited. In panel (b), the blue nodes represent the synchronous coherent part, the grey cells indicate the positions where the hub-reflected waves collide with an opposite wave from other paths, and the purple ones are the neighbors of the hub with antiphased oscillation. (c) The time series of the hub node $i = 3$ and one of its antiphased neighbor cells $i = 155$. (d) The evolution of the phase differences between the hub node $i = 3$ and its three typical neighbors $i = 66, 75$, and 155, which are defined as $\triangle\phi_i = \phi_3 - \phi_i$ ($i = 66, 75$, and 155). The light grey dashed rectangles in (c) and (d) denote the period in which the hub is in the rest state prior to the next stimulation.

found that the hub receives the excitable waves propagated from all its neighbor nodes (denoted by the pink arrowed lines) in this stage. Under the coherent stimulations from these upstream driving neighbors, the hub can perform a suprathreshold excitation. On the other hand, Fig. 3(b) exhibits a completely different improved DPAD pattern after the hub node is aroused. It is shown that the excitable waves now propagate from the hub to its neighbor nodes and then the entire network as the hub experiences a firing (also demonstrated by the pink arrowed lines). Therefore, the hub behaves as a mirror to reflect the excitable waves. Some of these reflected outward waves arouse incoherent nonsynchronous cells (indicated by the red circles), while the others inspire

the downstream coherent synchronous ones (marked by the blue circles). The grey cells indicate the positions where the hub-reflected waves collide with an opposite wave from other paths.

In addition, the two nodes $i = 150$ and 155 labeled in purple can also be observed, which are the neighbor cells of the hub with antiphased oscillation. Here we use the neighbor $i = 155$ to further explain the key factor of these anti-phased cells in sustaining the CLOM. Fig. 3(c) shows the time series of the hub node $i = 3$ and the neighbor cell $i = 155$. By comparing with that of the other neighbors, such as the blue neighbor $i = 66$ and the green neighbor $i = 75$ displayed in Fig. 2(f), the purple neighbor $i = 155$ can undergo an extra

excitation during the rest state of the hub, which is denoted by the light grey dashed rectangle. This means that, during the rest period of the hub prior to the next stimulation, the neighbor cell $i = 155$ can execute an antiphased oscillation and sustain the system. To explore the phase relation between the hub and its neighbors explicitly, the evolutions of the phase differences between the hub node $i = 3$ and its three typical neighbors (i.e., the cells $i = 66$, 75, and 155) are exhibited in Fig. 3(d). It is shown clearly that, during the rest period of the hub, only the purple neighbor $i = 155$ is antiphased (also indicated by the light grey dashed rectangle). Due to the existence of these few antiphased cells in the incoherent part, several hub-reflected waves can survive in the process of wave collisions, and can propagate back from all around to intrigue the hub again as Fig. 3(a). The combination of the hub and these antiphased neighbors provides a deterministic mechanism in sustaining the nonsynchronous oscillation.

The above two distinct excitation processes exposed in Fig. 3 also lead to an interesting consequence that the incoherent nonsynchronous cells can be stimulated twice in one period, while the coherent synchronous nodes experience only one fire. This well interprets the coexistence of two distinct dynamical modes in one system shown in Figs. 2(e) and 2(f), which forms the CLOM in the ESFN.

It is necessary to reflect on the studies of sustained oscillation in excitable networks and make a comparison of the present mechanism with previous explorations. The heterogeneity property in networks usually prevents the sustained oscillatory dynamics and wave propagation. Therefore, this mechanism in sustaining the CLOM in excitable complex networks is completely different from the traditional periodic oscillation mechanism in excitable networks discussed before [15], where the Winfree loop serves as the source in maintaining the NOM with a single dynamical behavior. This explains why this kind of CLOM can not be observed in homogeneous excitable networks.

It is important to study the robustness of this topological-heterogeneity induced CLOM in the ESFNs. To test this, we further modify the network topology by discarding one of the upstream driving neighbors, e.g., the green cell $i = 75$, from the minimal network Fig. 2(c). This operation is implemented at $t = 1000$, which is indicated by the light grey dashed lines in Figs. 4(a) and 4(b), where the spatiotemporal pattern and the time series of the other three highlighted cells are, respectively, displayed. The black regions in the pattern denote the rest state of the discarded cells. It is clearly shown that, as one of the upstream driving neighbors is deleted, the suprathreshold excitation of the hub will stop. This can be clearly seen from the disappearance of the red-lined firings in the spatiotemporal pattern of Fig. 4(a) and the dynamical transitions of u_3 and u_{66} from the suprathreshold excitation to the subthreshold vibration shown in Fig. 4(b). Although the oscillation of the network still persists, the hub-intrigued large-amplitude firings of the original downstream coherent synchronous cells are suppressed immediately. Furthermore the dynamical behaviors of those nonsynchronous cells are also modulated [see the orange trajectory of u_{89} in Fig. 4(b)], from the period-2 excitation to the regular period-1 excitation.

Figure 4(c) displays the mean phase velocity profile $\{\omega_i\}$ corresponding to Fig. 4(a). By comparing this profile with
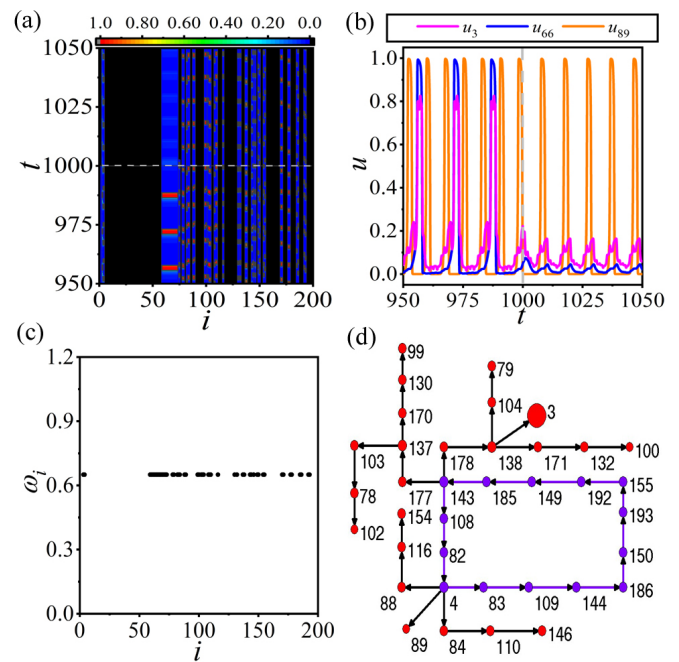

FIG. 4. (a), (b) The spatiotemporal evolution pattern [(a)] and the time series of the other three highlighted cells [(b)] as the green upstream driving neighbor $i = 75$ of the hub is discarded from the minimal scale-free structure of Fig. 2(c). This option is implemented at $t = 1000$, which is denoted by the light grey dashed line. The CLOM of Fig. 2(d) is reduced to the traditional *normal oscillation mode* (NOM) with a single dynamical behavior. (c), (d) The mean phase velocity profile $\{\omega_i\}$ [(c)] and the unique DPAD pattern [(d)] of this NOM.

that shown in Fig. 2(e), the two-band frequency distribution merges into a unique frequency band. This further confirms that, as the excitations received by the hub from the upstream driving neighbors are weakened by deleting an upstream node, the topological-heterogeneity induced CLOM in the ESFN is reduced to the traditional NOM with a single dynamical mode. Figure 4(d) presents the DPAD pattern of this NOM, which possesses a Winfree loop (labeled by the pink ring) as the source maintaining the oscillation. This is in sharp contrast to the doubly switched DPAD patterns of the CLOM in Figs. 3(a) and 3(b). The above discussions reveal that the PADs of hub (called the resultant drive in the following) from the upstream driving neighbors need to accumulate to a critical threshold, beyond which the hub can implement a suprathreshold excitation to intrigue the downstream coherent synchronous part. This incorporates with the topology heterogeneity to form the CLOM in the ESFN.

V. THE EFFECTIVE-DRIVING APPROACH

To understand how the accumulated drive received by the hub facilitates the formation of the CLOM in the ESFN and to expose the corresponding critical drive, an analysis that is independent of specific network structures is necessary. The above discussions indicate that all the coherent synchronous cells in the ESFN are connected directly to the hubs, and those cells in the CLOMs are also excited by these hubs, i.e.,

become the downstream nodes of the hubs. This is exactly caused by the topology heterogeneity of scale-free networks and, importantly, is the mechanism in forming the CLOM in the ESFN. This inspires us to consider the following empirical model consisting of a *downstream synchronous cell* (DSC) connecting with k^{DSC} hubs. A schematic diagram of this model is illustrated in Fig. 5(a), where each hub receives an independent effective resultant drive that equivalently presents the accumulative PADs from its upstream driving neighbors in real networks. The dynamical equations of the activation variables of the DSC u^{DSC} and the ith hub u_i^{hub} can be written as

$$\frac{du^{DSC}}{dt} = \frac{1}{\varepsilon} u^{DSC}(1 - u^{DSC})\left(u^{DSC} - \frac{v^{DSC} + b}{a}\right)$$
$$+ D\left(\sum_{i=1}^{k^{DSC}} u_i^{hub} - k^{DSC} u^{DSC}\right), \qquad (5)$$

$$\frac{du_i^{hub}}{dt} = \frac{1}{\varepsilon} u_i^{hub}(1 - u_i^{hub})\left(u_i^{hub} - \frac{v_i^{hub} + b}{a}\right)$$
$$+ D\left(F_i - k_i^{hub} u_i^{hub}\right). \qquad (6)$$

Here the subscript $i = 1, 2, \ldots, k^{DSC}$ labels the ith hub, and the time-dependent term $F_i(t)$ implies the equivalent resultant drive received by the ith hub. k^{DSC} and k_i^{hub}, respectively, represent the degrees of the DSC and the ith hub. The corresponding recovery variables v^{DSC} and v_i^{hub} still follow Eq. (2).

The key point of the simplified model Eqs. (5) and (6) can be understood as follows. Suppose a hub receives an equivalent resultant drive from its upstream driving neighbors—this will change its dynamical behavior. As long as the resultant drive surpasses a critical value, the hub will be excited. This will consequently stimulate its downstream cells to experience a coherent and synchronous firing. By combining with the incoherent nonsynchronous oscillations, a coexisting coherent-incoherent CLOM will eventually emerge in the network. This indicates that the transition to the suprathreshold excitation of the hub and its critical threshold is the key point. Based on Eqs. (5) and (6), we can conveniently unfold this issue by effectively working out the necessary condition for the emergence of the CLOM in the network according to the resultant drive. Most importantly, this analysis is irrelevent of network topology and applicable to various types of networks.

Enlightened by the features of resultant drives received by hubs in networks, one empirically constructs the following effective driving $F_i(t)$ to mimic the resultant drive received by the ith hub:

$$F_i(t) = \begin{cases} \left(\frac{1}{3}F_i^{max} - f_i^0\right)\sin\left[2\pi\frac{5}{4T}t\right] + f_i^0 & (0 \leqslant t \leqslant \frac{1}{3}T_i) \\ \left(\frac{2}{3}F_i^{max} - f_i^1\right)\sin\left[2\pi\frac{5}{4T}\left(t - \frac{1}{3}T_i\right)\right] + f_i^1 & \left(\frac{1}{3}T_i < t \leqslant \frac{2}{3}T_i\right) \\ \left(F_i^{max} - f_i^2\right)\sin\left[2\pi\frac{5}{4T}\left(t - \frac{2}{3}T_i\right)\right] + f_i^2 & \left(\frac{2}{3}T_i < t \leqslant T_i\right) \\ 0 & t > T_i, \end{cases} \qquad (7)$$

where

$$f_i^1 = F_i\left(\frac{1}{3}T_i\right) \quad \text{and} \quad f_i^2 = F_i\left(\frac{2}{3}T_i\right). \qquad (8)$$

In Eq. (7), the baseline f_i^0, the amplitude F_i^{max}, and the duration T_i are three key control parameters that can determine

the form of function $F_i(t)$, which can effectively mimic diverse resultant drives received by hubs in practice. Figure 5(b) presents the time series of the resultant drive $F_i(t)$ for $f_i^0 = 1.0$, $F_i^{max} = 20$ and $T_i = 70$. In the following, we will focus on how these vital parameters impact the excitation of the DSC, and give the critical threshold for the formation of the CLOM.

Let us reveal the predictable parameter regions of CLOM by analyzing Eqs. (5) and (6) for different network parameters and diverse forms of the resultant drives. The results are presented in Fig. 6 as phase diagrams in the (T_i, F_i^{max}) plane for different situations. The white regions denote the parameters (T_i, F_i^{max}) where the DSC can be excited and the CLOM can form in an excitable complex network. In the grey region, the DSC fails to be excited, and only an incoherent NOM emerges.

Figures 6(a)–6(c) present the phase diagrams for only one hub in the network with degrees $k_1^{hub} = 25$ [Fig. 6(a)], $k_1^{hub} = 50$ [Fig. 6(b)], $k_1^{hub} = 75$ [Fig. 6(c)], and $k^{DSC} = 1$, $f_1^0 = 0$. This case is similar to the two reduced minimal network topologies shown in Figs. 2(a) and 2(c). It can be found that as the degree of the hub increases, the white firing regions as well as the CLOM domains shrink dramatically, i.e., a larger amplitude and longer duration of the resultant drive are needed to form the CLOM. This means that a higher degree of topology heterogeneity is adverse to the formation of CLOM
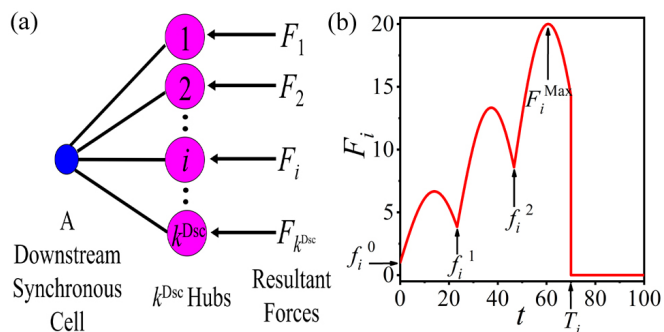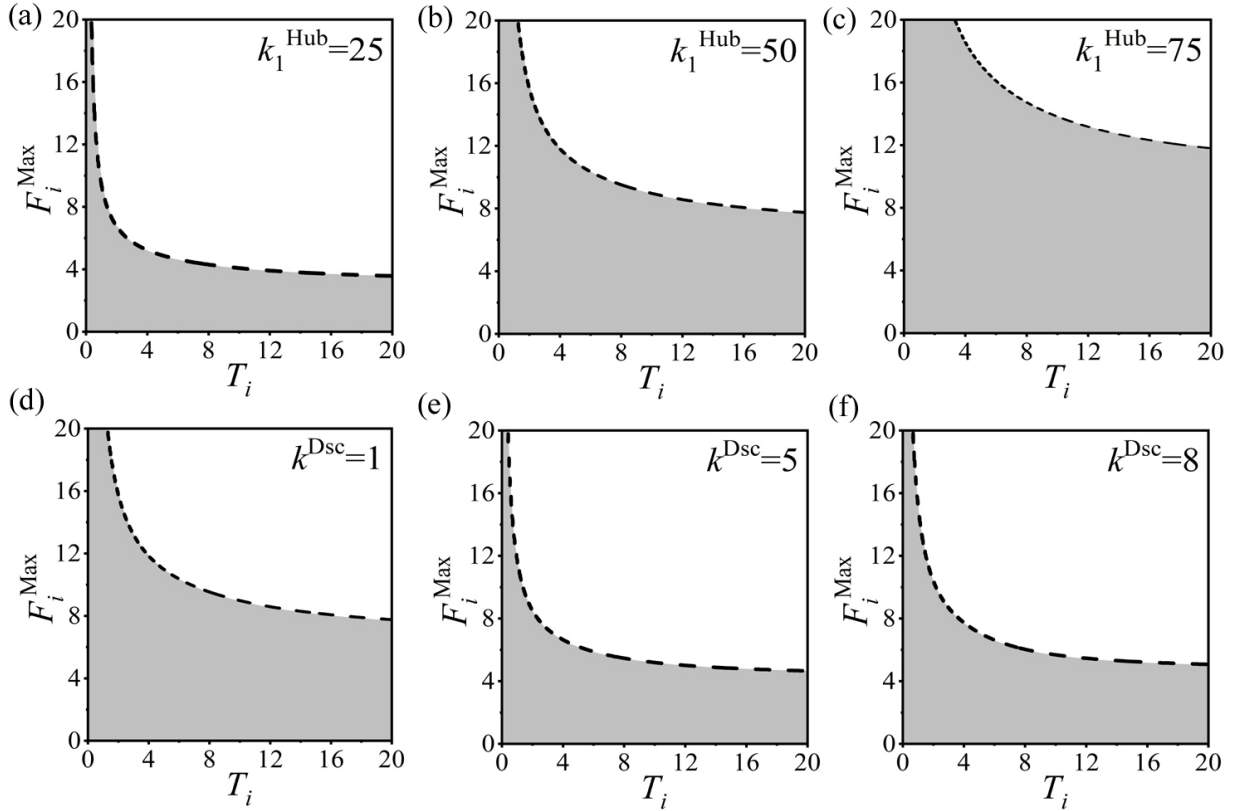

FIG. 5. (a) The schematic diagram of the effective-driving approach, which consists of a *downstream synchronous cell* (DSC) connecting with k^{DSC} hubs. Each hub receives an independent resultant drive $F_i(t)$ representing the accumulative PADs from its upstream driving neighbors in real networks. (b) The time series of the resultant drive $F_i(t)$ for $f_i^0 = 1.0$, $F_i^{max} = 20$, and $T_i = 70$.

FIG. 6. The phase diagrams in the $(T_i, F_i^{\max})$ plane for different situations. Each phase plane is split by the black dash boundary into two distinct parameter domains, i.e., the CLOM regions (white) and the NOM regions (grey). (a)–(c) For different hub degrees $k_1^{\text{hub}} = 25$ [(a)], $k_1^{\text{hub}} = 50$ [(b)], $k_1^{\text{hub}} = 75$ [(c)], with $k^{\text{DSC}} = 1$ and $f_1^0 = 0$. (d)–(f) For different DSC degrees $k^{\text{DSC}} = 1$ [(d)], $k^{\text{DSC}} = 5$ [(e)], $k^{\text{DSC}} = 8$ [(f)], with $k_i^{\text{hub}} = 50$ and $f_i^0 = 0$.

in the network. Figures 6(d)–6(f) exhibit the influence of the degree of DSC for $k^{\text{DSC}} = 1$ [Fig. 6(d)], $k^{\text{DSC}} = 5$ [Fig. 6(e)] and $k^{\text{DSC}} = 8$ [Fig. 6(f)] with $k_i^{\text{ubhub}} = 50$ and $f_i^0 = 0$, where the CLOM regime first increases and then decreases with increasing k^{DSC}, implying an optimal k^{DSC} that facilitates the emergence of CLOMs, i.e., a moderate number of hubs in a network is helpful to the formation of the CLOMs in the ESFN.

Now let us test the validity of this effective-driving approach by analyzing the above several cases. For the minimal scale-free network of Fig. 2(c), the topology parameters in the effective-driving method are $k^{\text{DSC}} = 1$ and $k_1^{\text{hub}} = 27$. Figure 7(a) displays the time series of the effective resultant drive received by the hub node $i = 3$. It is shown that $F_1(t)$ oscillates periodically in a wide range. The baseline f_1^0 and the amplitude $F_1^{\max}$ are, respectively, given as the minimum (denoted by blue circle) and the maximum (indicated by green square) values of $F_1(t)$ before the DSC fires in one oscillation period. Moreover, based on the driving function $F(t)$ in Eq. (7), the duration can be approximatively identified as $T_1 = \frac{15}{13} * (t_2 - t_1)$, where $F_1(t_1) = f_1^0$ and $F_1(t_2) = F_1^{\max}$. In Fig. 7(b), we plot the phase diagram $(T_1, F_1^{\max})$ by adopting these parameters and label the values of $T_1 \approx 10.06$ and $F_1^{\max} \approx 4.94$ by using the red cross. The present case clearly shows that the actual resultant drive $F_1(t)$ received by the hub is located in the white firing region, indicating that the CLOM can emerge in the network shown in Fig. 2(c).

A similar test can also be carried out for the case given in Fig. 4. The time series of the effective resultant drive and the CLOM regions by discarding the upstream driving neighbor $i = 75$ at $t = 1000$ (see the grey dashed line) are, respectively, displayed in Figs. 7(c) and 7(d). It is shown that the driving $F_1(t)$ changes dramatically as cell $i = 75$ is deleted and falls into the grey domain [see the red cross $(T_1, F_1^{\max}) \approx (6.32, 3.67)$]. This means that as one of the upstream driving neighbors of the hub is eliminated, the new PADs now cannot surpass the critical threshold to excite the DSC. As a result, the original CLOM degenerates and the system evolves to a NOM, which agrees with the results shown in Fig. 4.

Let us further try to analyze the original scale-free network with multiple hubs shown in Fig. 1, for which the DSC is connected to $k^{\text{DSC}} = 2$ hubs with degrees $k_1^{\text{hub}} = 93$ and $k_2^{\text{hub}} = 133$. The resultant drives received by these two hubs are also different and displayed by the pink [$F_1(t)$] and purple [$F_2(t)$] curves in Fig. 7(e), respectively. In this case, we use $F(t) = F_1(t) + F_2(t)$ (red curve) to select the moments t_1 and t_2 for the minimum and the maximum values of $F(t)$ before the DSC fires in one period [$F_{1,2}(t_1) = f_{1,2}^0$ and $F_{1,2}(t_2) = F_{1,2}^{\max}$]. Figure 7(f) exposes the CLOM domains in the $(F_1^{\max}, F_2^{\max})$ parameter plane. The actual resultant drives received by these two hubs in the original ESFN of Fig. 1 are $(F_1^{\max}, F_2^{\max}) \approx (13.33, 16.83)$ (see the red cross), which falls in the white firing region. This confirms the emergence of the CLOM in the ESFN of Fig. 1.
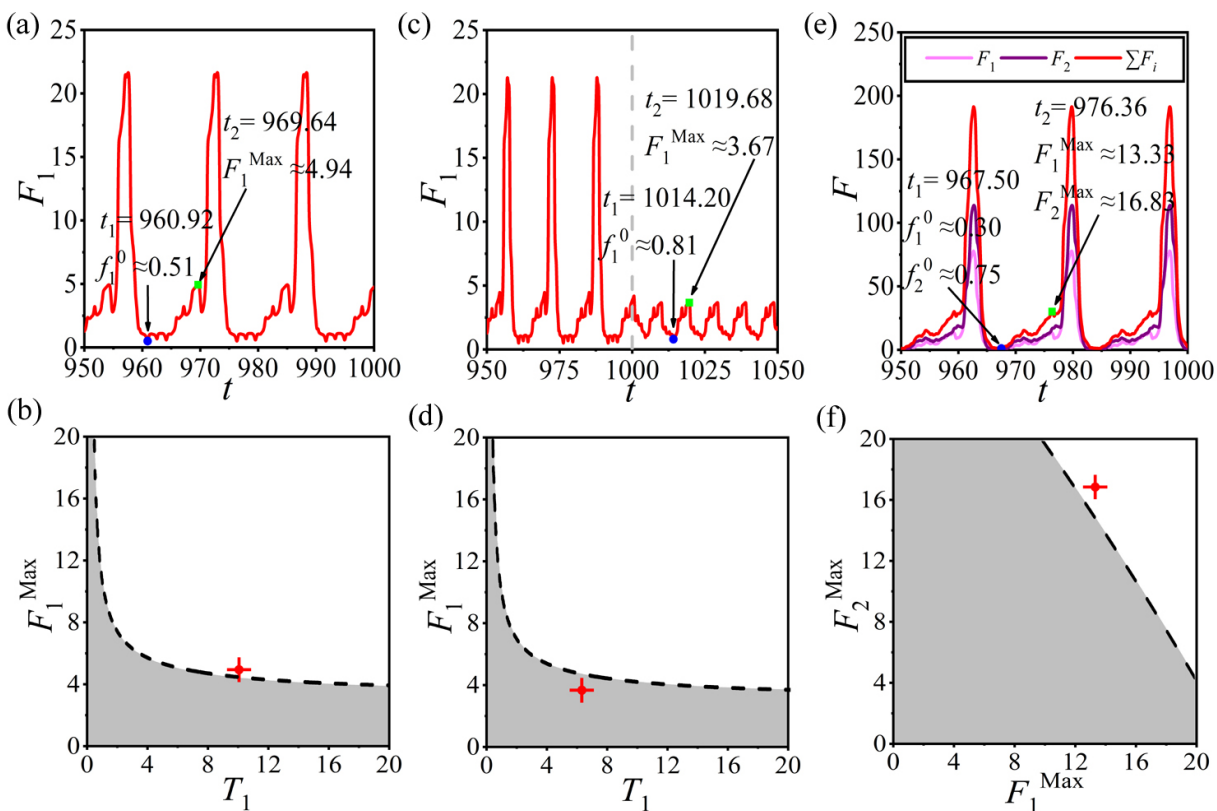
FIG. 7. The time series of the effective resultant drives received by the hubs [(a), (c), (e)] and the corresponding CLOM (white) and NOM regions (grey) [(b), (d), (f)] for the three real cases illustrated in the present paper. (a), (b) For the CLOM on the minimal scale-free structure of Figs. 2(c) and 2(d). (c), (d) For the NOM of Fig. 4. (e), (f) For the CLOM in the original ESFN of Fig. 1. The red crosses in panels (b), (d), (f) represent the actual resultant drives received by the hubs in these three cases.

The above examples strongly support the validity and applicability of the effective-driving approach we proposed here. The present empirical method cannot only judge whether the CLOM may emerge in excitable complex networks but also predict the critical threshold for the formation of the CLOM.

VI. CONCLUSION

To summarize, in this paper, CLOM dynamics in the ESFNs without rotational coupling scheme is reported. It is found that CLOMs can emerge as a coexistence of coherent synchronous firings and incoherent nonsynchronous oscillations. To explore the mechanism of this kind of CLOM, we propose a topology-reduction scheme to simplify the network to a minimal structure containing a unique hub by preserving the CLOMs with coexisting coherent and incoherent segments. Specifically, the coherent cells on the minimal network can execute synchronous firings with a basic frequency, while the incoherent ones perform nonsynchronous oscillations around the doubling frequency. In terms of the extended DPAD method, the mechanism of the emergence of CLOM in the ESFN is discussed in detail, by which the topology heterogeneity is revealed as the mechanism in forming and maintaining the CLOM. The hub acts not only as a mirror to reflect the waves exciting the incoherent part to sustain the nonsynchronous oscillations permanently but also as the source to intrigue the downstream synchronous coherent part firings to form the CLOM in the ESFN.

The topological mechanism presented in this paper is a unique mechanism in forming the CLOM in excitable complex networks. This can help us understand competitions and self-organizations of NOM and CLOM in excitable systems with topological homogeneity and heterogeneity. As a comparison, our extensive explorations indicate that the CLOMs cannot emerge in homogeneous networks such as ER random networks, homogeneous random networks, and small-world networks. Topological heterogeneity is the indispensible ingredient in supporting the coexistence of coherence and incoherence.

An effective-driving approach is proposed to theoretically analyze the CLOM in excitable complex networks, which consists of a DSC connecting with k^{DSC} hubs. An empirical drive function $F(t)$ is proposed to mimic the effective resultant drive received by the hub, which is equivalent to the PADs from the corresponding upstream driving neighbors in real networks. Based on this analysis method, one cannot only judge whether the CLOM may emerge in excitable complex networks but also predict the critical threshold for the formation of the CLOM. More importantly, this effective-driving approach is irrelevant of network topology and can be applied to various types of networks. The coincidence of the theoretical predictions and the numerical results in real cases with different situations further confirms the validity and applicability of the analysis we proposed here.

Recently, more and more human neuroimaging data obtained from structural magnetic resonance imaging, functional

magnetic resonance imaging, electroencephalography, and magnetoencephalography confirmed that the structural and functional brain networks usually have community features, small-world properties, and heavy-tailed degree distributions [45–49]. This kind of organization in brain networks is the result of the economic principle of cost-efficiency trade-off between the physical cost of the network and the information integration among whole brain system [50]. Considering the network wiring-cost premium, brain networks tend to organize community (module) structures to perform specific functions. To achieve global information integration of functionally specialized brain regions located far apart from each other in anatomical space, localized communities (modules) are topologically organized by long-distance axonal projections, which does exhibit the small-world property. To significantly improve the integration efficiency, i.e., achieving the high global efficiency of information transfer across the whole brain network, long-distance connections between spatially remote functional communities (modules) preferentially link to the regions with large degrees. This forms hub regions in brain networks, such as parts of medial parietal cortex, cingulate cortex, and superior frontal cortex.

More importantly, these hub regions are often the parts of a multimodal association cortex.

In this paper, we systematically investigated the CLOMs emerging in ESFNs and exposed the determinant of topology heterogeneity (i.e., the hubs) in forming the CLOM. As we know, the CLOM, as one of the most important rhythm modes, can self-organize to emerge in brains with different scales. It is functionally related to some vital physiological processes in human beings, such as the first-night effect and epileptic seizures, for typical examples. The topological-heterogeneity induced CLOMs presented in this paper may shed light on a deep comprehension of these amazing modes in the highly complex and heterogeneous brain networks.

[1] E. Meron, Pattern formation in excitable media, Phys. Rep. **218**, 1 (1992).

[2] C. Cross and P. C. Hoheberg, Pattern formation outside of equilibrium, Rev. Mod. Phys. **65**, 851 (1993).

[3] W. M. Usrey and R. C. Reid, Synchronous activity in the visual system, Annu. Rev. Physiol. **61**, 435 (1999).

[4] M. Stopfer, S. Bhagavan, B. H. Smith, and G. Laurent, Impaired odour discrimination on desynchronization of odour-encoding neural assemblies, Nature **390**, 70 (1997).

[5] L. M. Ward, Synchronous neural oscillations and cognitive processes, Trends Cognit. Sci. **7**, 553 (2003).

[6] M. Steriade, D. A. McCormick, and T. J. Sejnowski, Thalamocortical oscillations in the sleeping and aroused brain, Science **262**, 679 (1993).

[7] A. Roxin, H. Riecke, and S. A. Solla, Self-Sustained Activity in a Small-World Network of Excitable Neurons, Phys. Rev. Lett. **92**, 198101 (2004).

[8] S. Sinha, J. Saramäki, and K. Kaski, Emergence of self-sustained patterns in small-world excitable media, Phys. Rev. E **76**, 015101(R) (2007).

[9] W. Gu, X. Liao, L. Zhang, X. Huang, G. Hu, and Y. Mi, Synchronous firings in small-world networks of excitable nodes, Europhys. Lett. **102**, 28001 (2013).

[10] P. McGraw and M. Menzinger, Self-sustaining oscillations in complex networks of excitable elements, Phys. Rev. E **83**, 037102 (2011).

[11] N. E. Kouvaris, T. Isele, A. S. Mikhailov, and E. Schöll, Propagation failure of excitation waves on trees and random networks, Europhys. Lett. **106**, 68001 (2014).

[12] T. Isele and E. Schöll, Effect of small-world topology on wave propagation on networks of excitable elements, New J. Phys. **17**, 023058 (2015).

[13] C. Fretter, A. Lesne, C. C. Hilgetag, and M. T. Hütt, Topological determinants of self-sustained activity in a simple model of excitable dynamics on graphs, Sci. Rep. **7**, 42340 (2017).

[14] J. Danison and M. Perez, Complex self-sustained oscillation patterns in modular excitable networks, Phys. Rev. E **98**, 042308 (2018).

[15] Y. Qian, X. Huang, G. Hu, and X. Liao, Structure and control of self-sustained target waves in excitable small-world networks, Phys. Rev. E **81**, 036101 (2010).

[16] Y. Qian, Emergence of self-sustained oscillations in excitable Erdös-Rényi random networks, Phys. Rev. E **90**, 032807 (2014).

[17] Y. Qian, G. Zhang, Y. Wang, C. Yao, and Z. Zheng, Winfree loop sustained oscillation in two-dimensional excitable lattices: Prediction and realizations, Chaos **29**, 073106 (2019).

[18] Y. Qian, C. Zhang, Z. Wei, F. Liu, C. Yao, and Z. Zheng, The optimal oscillation mode in excitable small-world networks, Europhys. Lett. **131**, 38002 (2020).

[19] Y. Qian, Z. Lei, Z. Wei, X. Cui, C. Zhang, and Z. Zheng, The oscillation-mode dynamics in excitable complex networks: Transfer and transition, Europhys. Lett. **135**, 48001 (2021).

[20] Z. Lei, J. Liu, Y. Zhao, F. Liu, Y. Qian, and Z. Zheng, New burst-oscillation mode in paced one-dimensional excitable systems, Front. Physiol. **13**, 854887 (2022).

[21] Z. Wang and Z. Liu, A brief review of chimera state in empirical brain networks, Front. Physiol. **11**, 724 (2020).

[22] F. Parastesh, S. Jafari, H. Azarnoush, Z. Shahriari, Z. Wang, S. Boccaletti, and M. Perc, Chimeras, Phys. Rep. **898**, 1 (2021).

[23] Y. Kuramoto and D. Battogtokh, Coexistence of coherence and incoherence in nonlocally coupled phase oscillators, Nonlinear Phenom. Complex Syst. **5**, 380 (2002).

[24] I. Omelchenko, Y. L. Maistrenko, P. Hövel, and E. Schöll, Loss of Coherence in Dynamical Networks: Spatial Chaos and Chimera States, Phys. Rev. Lett. **106**, 234102 (2011).

[25] I. Omelchenko, B. Riemenschneider, P. Hövel, Y. L. Maistrenko, and E. Schöll, Transition from spatial coherence

to incoherence in coupled chaotic systems, Phys. Rev. E **85**, 026212 (2012).

[26] B. K. Bera, D. Ghosh, and M. Lakshmanan, Chimera states in bursting neurons, Phys. Rev. E **93**, 012205 (2016).

[27] I. A. Shepelev, T. E. Vadivasova, A. V. Bukh, G. I. Strelkova, and V. S. Anishchenko, New type of chimera structures in a ring of bistable FitzHugh-Nagumo oscillators with nonlocal interaction, Phys. Lett. A **381**, 1398 (2017).

[28] Z. Lei, S. Pu, H. Zhang, C. Yao, Y. Qian, and Z. Zheng, Bistability-induced chimeras in one-dimensional paced excitable rings with nonlocal couplings, Europhys. Lett. **139**, 62001 (2022).

[29] D. M. Abrams, R. Mirollo, S. H. Strogatz, and D. A. Wiley, Solvable Model for Chimera States of Coupled Oscillators, Phys. Rev. Lett. **101**, 084103 (2008).

[30] E. A. Martens, C. R. Laing, and S. H. Strogatz, Solvable Model of Spiral Wave Chimeras, Phys. Rev. Lett. **104**, 044101 (2010).

[31] S. R. Ujjwal and R. Ramaswamy, Chimeras with multiple coherent regions, Phys. Rev. E **88**, 032902 (2013).

[32] A. Zakharova, M. Kapeller, and E. Schöll, Chimera Death: Symmetry Breaking in Dynamical Networks, Phys. Rev. Lett. **112**, 154101 (2014).

[33] U. K. Verma and G. Ambika, Amplitude chimera and chimera death induced by external agents in two-layer networks, Chaos **30**, 043104 (2020).

[34] G. G. Mascetti, Unihemispheric sleep and asymmetrical sleep: Behavioral, neurophysiological, and functional perspectives, Nat. Sci. Sleep **8**, 221 (2016).

[35] M. Tamaki, J. W. Bang, and T. Watanabe, Night watch in one brain hemisphere during sleep associated with the first-night effect in humans, Curr. Biol. **26**, 1190 (2016).

[36] M. Gerster, R. Berner, J. Sawicki, A. Zakharova, A. škoch, J. Hlinka, K. Lehnertz, and E. Schöll, FitzHugh-Nagumo oscillators on complex networks mimic epileptic-seizure-related synchronization phenomena, Chaos **30**, 123130 (2020).

[37] M. S. Santos, J. D. Szezech, F. S. Borges, K. C. Iarosz, I. L. Caldas, A. M. Batista, R. L. Viana, and J. Kurths, Chimera-like states in a neuronal network model of the cat brain, Chaos Solitons Fractals **101**, 86 (2017).

[38] J. Tang, J. Zhang, J. Ma, and J. Luo, Noise and delay sustained chimera state in small world neuronal network, Sci. China Technol. Sci. **62**, 1134 (2019).

[39] S. Majhi, B. K. Bera, D. Ghosh, and M. Perc, Chimera states in neuronal networks: A review, Phys. Life Rev. **28**, 100 (2019).

[40] H. M. Mitchell, P. S. Dodds, J. M. Mahoney, and C. M. Danforth, Chimera states and seizures in a mouse neuronal model, Int. J. Bifurcation Chaos **30**, 2050256 (2020).

[41] S. Huo, C. Tian, M. Zheng, S. Guan, C. Zhou, and Z. Liu, Spatial multi-scaled chimera states of cerebral cortex network and its inherent structure-dynamics relationship in human brain, Natl. Sci. Rev. **8**, nwaa125 (2021).

[42] M. Bär and M. Eiswirth, Turbulence due to spiral breakup in a continuous excitable medium, Phys. Rev. E **48**, R1635 (1993).

[43] A.-L. Barabási and R. Albert, Emergence of scaling in random networks, Science **286**, 509 (1999).

[44] I. Omelchenko, E. Omelchenko, P. Hövel, and E. Schöll, When Nonlocal Coupling Between Oscillators Becomes Stronger: Patched Synchrony or Multichimera States, Phys. Rev. Lett. **110**, 224101 (2013).

[45] V. M. Eguíluz, D. R. Chialvo, G. A. Cecchi, M. Baliki, and A. V. Apkarian, Scale-Free Brain Functional Networks, Phys. Rev. Lett. **94**, 018102 (2005).

[46] P. Bonifazi, M. Goldin, M. A. Picardo, I. Jorquera, A. Cattani, G. Bianconi, A. Represa, Y. Ben-Ari, and R. Cossart, GABAergic hub neurons orchestrate synchrony in developing hippocampal networks, Science **326**, 1419 (2009).

[47] M. P. van den Heuvel and O. Sporns, Rich-club organization of the human connectome, J. Neurosci. **31**, 15775 (2011).

[48] M. P. van den Heuvel, R. S. Kahn, J. Goñi, and O. Sporns, High-cost, high-capacity backbone for global brain communication, Proc. Natl. Acad. Sci. USA **109**, 11372 (2012).

[49] M. P. van den Heuvel and O. Sporns, Network hubs in the human brain, Trends Cognit. Sci. **17**, 683 (2013).

[50] E. Bullmore and O. Sporns, The economy of brain network organization, Nat. Rev. Neurosci. **13**, 336 (2012).